

Review

Research Progress on Preparation Methods of Skutterudites

Chengyu Zhao ^{1,2}, Minhua Wang ³ and Zhiyuan Liu ^{1,2,*} 

¹ Key Laboratory of Green Fabrication and Surface Technology of Advanced Metal Materials, Ministry of Education, Anhui University of Technology, Maanshan 243002, China; 13030610154@163.com

² School of Materials Science and Engineering, Anhui University of Technology, Maanshan 243002, China

³ School of Foreign Languages, Anhui University of Technology, Maanshan 243002, China; m19159354437@163.com

* Correspondence: zhiyuanliu826@ahut.edu.cn

Abstract: Thermoelectric material is a new energy material that can realize the direct conversion of thermal energy and electric energy. It has important and wide applications in the fields of the recycling of industrial waste heat and automobile exhaust, efficient refrigeration of the next generation of integrated circuits and full spectrum solar power generation. Skutterudites have attracted much attention because of their excellent electrical transport performance in the medium temperature region. In order to obtain skutterudites with excellent properties, it is indispensable to choose an appropriate preparation method. This review summarizes some traditional and advanced preparation methods of skutterudites in recent years. The basic principles of these preparation methods are briefly introduced. Single-phase skutterudites can be successfully obtained by these preparation methods. The study of these preparation methods also provides technical support for the rapid, low-cost and large-scale preparation of high-performance thermoelectric materials.

Keywords: thermoelectric materials; skutterudites; preparation methods; thermoelectric properties



Citation: Zhao, C.; Wang, M.; Liu, Z. Research Progress on Preparation Methods of Skutterudites. *Inorganics* **2022**, *10*, 106. <https://doi.org/10.3390/inorganics10080106>

Academic Editors: Marco Fronzi, Paolo Mele and Giovanna Latronico

Received: 4 July 2022

Accepted: 21 July 2022

Published: 26 July 2022

Publisher's Note: MDPI stays neutral with regard to jurisdictional claims in published maps and institutional affiliations.



Copyright: © 2022 by the authors. Licensee MDPI, Basel, Switzerland. This article is an open access article distributed under the terms and conditions of the Creative Commons Attribution (CC BY) license (<https://creativecommons.org/licenses/by/4.0/>).

1. Introduction

The global consumption of nonrenewable energy is increasing rapidly and the total amount of energy consumed is more than half of the known reserves. If we do not carry out planned exploitation and develop new energy, the nonrenewable resources on the earth will be gradually exhausted [1]. With the overexploitation and use of underground energy, the carbon balance on the earth's surface has been broken, resulting in a series of environmental problems such as the greenhouse effect. Therefore, it is urgent to develop renewable and sustainable new energy. In addition, the maximum energy efficiency of engines is about 41% [2]. Most of the remaining energy is consumed in other forms and cannot be effectively utilized. Thermoelectric (TE) material is a kind of new energy functional material, which can directly convert electric energy and heat energy into each other using the Seebeck effect and the Peltier effect [3,4]. Therefore, TE materials can convert lost energy into electric energy for human use through the Seebeck effect. The TE conversion efficiency of devices made of TE materials is relatively low. To improve the conversion efficiency of devices, the key is to improve the TE figure of merit ZT of materials [5–8].

The expression of ZT is as follows:

$$ZT = \frac{\alpha^2 \sigma}{\kappa} T \quad (1)$$

where α is the Seebeck coefficient of the material ($\mu\text{V}/\text{K}$); T is the absolute temperature (K); σ is the conductivity of the material (S/m); and κ is the total thermal conductivity of the material ($\text{W}/\text{m}\cdot\text{K}$) (including electronic thermal conductivity κ_E and lattice thermal conductivity κ_L). From the above equation, in order to obtain a high ZT value, it is necessary to increase the power factor ($\alpha^2 \sigma$) while reducing the total thermal conductivity of the

material. Since an increase in the Seebeck coefficient of the material usually causes a decrease in the electrical conductivity, the electronic thermal conductivity and electrical conductivity are positively correlated. Therefore, the increase or decrease of one variable cannot simply be considered. How to ensure the increase of $\alpha^2\sigma$ and the decrease of thermal conductivity is the key to enhancing the ZT value of TE materials.

In the 1990s, Slack was the first to put forward the ideal concept of “phonon glass electronic crystal” [9]. Slack pointed out that high-performance TE materials should have the same low thermal conductivity as glass and the same high conductivity as crystals. Since then, people have successively discovered clathrates with this feature [9]. Skutterudites are materials with this typical cage structure [10–14]. Filling in the icosahedral gap consisting of 12 Sb atoms with other impurity atoms can achieve independent electron and phonon synergistic modulation and significantly enhance the TE properties of skutterudites. In recent years, skutterudites have been dramatically improved by doping the framework atoms or filling the icosahedral voids and introducing the nano inclusions, with ZT values increasing from 1.0 to about 2.0 [15–26]. Wang et al. [15] prepared $\text{Yb}_x\text{Co}_4\text{Sb}_{12}$ -filled skutterudite that could reach ZT values of about 1.5. The ZT value of polyatomic filled skutterudite $(\text{R, Ba, Yb})_y\text{Co}_4\text{Sb}_{12}$ ($\text{R} = \text{Sr, La, Mm, DD, SrMm, SrDD}$) prepared by Rogl et al. [16] can even reach about 2.0. In addition to enhancing their properties by means of optimized doping and filling, these skutterudite materials have been prepared using some suitable preparation methods to obtain rich microstructures with independent electronic and phonon synergistic regulation, resulting in high ZT values. Therefore, the preparation methods are crucial to obtain high-performance skutterudites. In this review, we summarize some conventional and advanced preparation methods for skutterudite materials in recent years (Figure 1). Using these preparation methods, better performance skutterudites were successfully obtained. The study of these preparation methods also provides technical support for the rapid and low-cost large-scale preparation of high-performance TE materials.

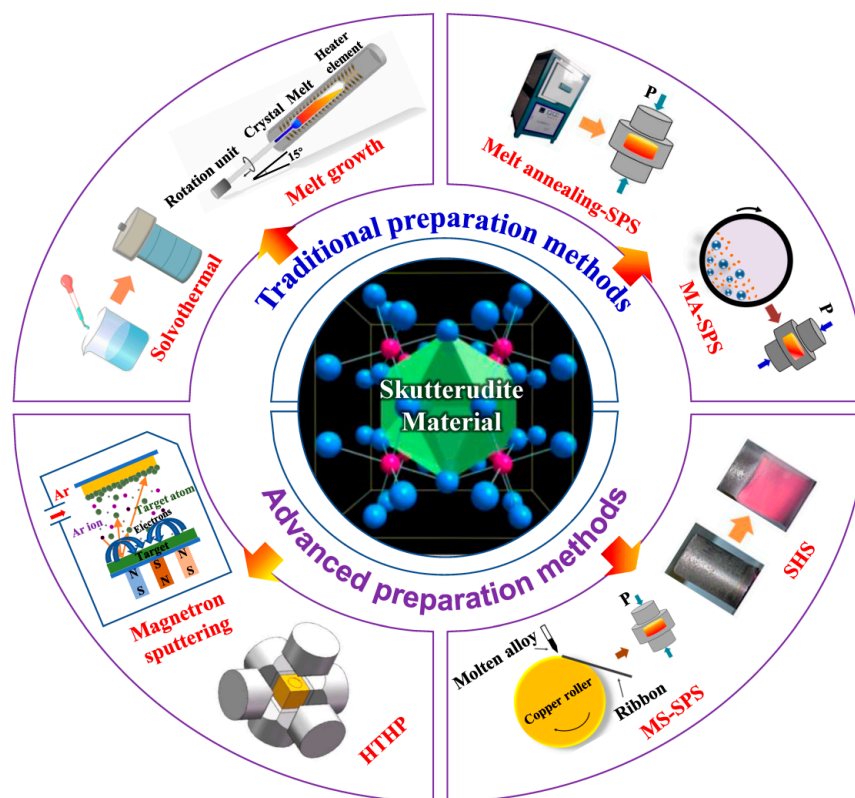


Figure 1. Schematic diagram of some preparation methods for skutterudite materials [27,28]. (MA: mechanical alloying; MS: melt spinning; SHS: self-propagating high-temperature synthesis; HTHP: high temperature and high pressure; SPS: spark plasma sintering).

2. Traditional Preparation Methods

2.1. Melt Growth Method

For the melt growth method, there is no destructive phase transition. Homo-component melted compounds or high-purity monomers with low vapor pressure/dissociation pressure are ideal materials for melt growth to obtain high-quality single crystals. Its growth process is accomplished by the movement of the solid–liquid interface, which is a directional solidification process under controlled conditions. Its quality is difficult to control because a finite solid solution is formed during its growth. In experiments, the required elements are often added in calculated proportions to obtain the target material after melting. This preparation method is also used to prepare skutterudite materials [28–30]. Pillaca et al. [28] successfully grew impurity-free single crystals of CoSb_3 using the tilted rotating Bridgman method (Figure 2a,b), whose single crystal growth was achieved in the high-temperature liquid phase with a high concentration of Sb. The single-phase CoSb_3 single crystals were finally prepared by first sealing the required raw materials in ampoules by mixing them thoroughly, followed by tilting the ampoules in a Bridgman-type crystal growth apparatus at an angle of 15° with respect to the horizon (Figure 2c), and finally by ramping up the cooling rate according to a constant rotation speed and temperature. Caillat et al. [29] prepared single crystals of the skutterudite phase using a melting vertical gradient cooling technique. The raw materials were sealed in a vacuum quartz tube in a certain ratio, melted and cooled by a melting furnace with a temperature difference, and finally, single-crystal CoSb_3 and RhSb_3 compounds were obtained.

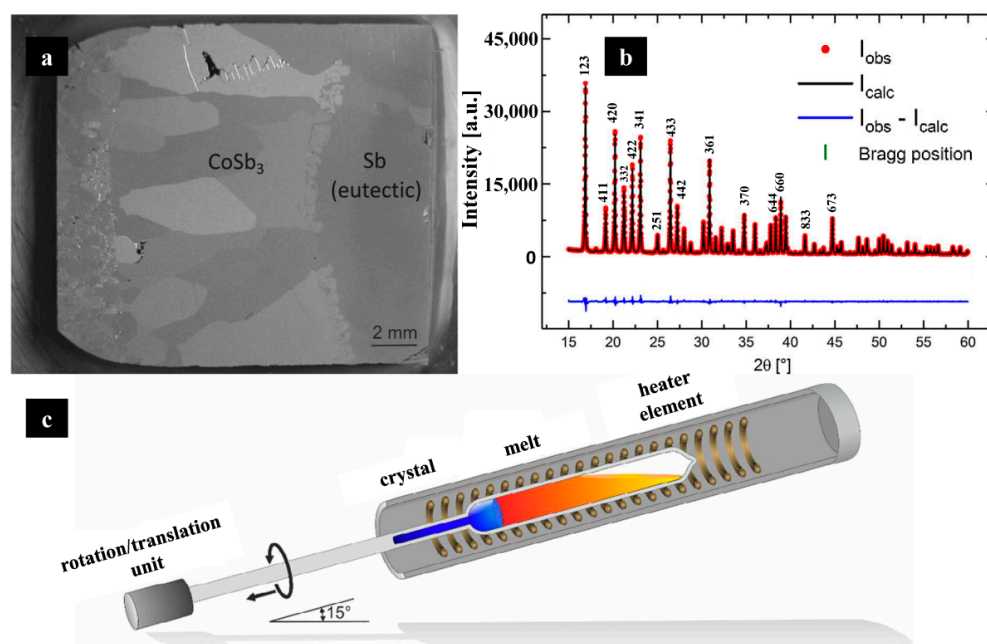


Figure 2. (a) Optical micrograph of the lapped surface of CoSb_3 ingot grown by the Inclined Rotary Bridgman method; (b) observed and calculated X-ray powder diffraction patterns of CoSb_3 ; (c) schematic of the apparatus used for the inclined Rotary Bridgman experiments [28].

2.2. Solvothermal Method

The solvothermal method is also known as the hydrothermal method. As the name implies, the chemical reaction is carried out under moist conditions. The specific implementation involves placing a certain proportion of high-purity raw materials together with the selected solvent in a reaction kettle. When the kettle is heated at the appropriate temperature, high temperature and pressure will be formed inside the kettle, which in turn will produce the desired target material. Since the ratio of reactants and the external environment can be controlled artificially, the advantages of this reaction are: the hydrothermal

method facilitates the control of the reaction kinetics and is more conducive to adjusting the shape and structure of the products; the solvothermal method generates materials with better crystallinity, faster reaction rate, and lower reaction temperature, which allows the synthesis of low-temperature isomers more easily. Therefore, this method is also used to prepare skutterudites [13,31–33]. One drawback of the solvent thermal method is that the yields of the prepared target materials are generally low, and further optimization of the conditions is needed to enhance the yields of the target products.

Qin et al. [31] used KOH, TeO₂, Co(NO₃)₂·6H₂O, SbCl₃, In(NO₃)₃·4.5H₂O as raw materials, KBH₄ as a reducing agent, and deionized water as solvent for hydrothermal synthesis at 180 °C for 48 h, followed by heat treatment and finally under vacuum to prepare bulk In-filled and Te-doped CoSb₃ samples by hot-press sintering at 650 °C for 80 MPa. The electrical transport properties showed that the longer annealed In-filled and Te-doped CoSb₃ samples had good electrical properties with the highest power factor of 38.4 μW·cm⁻¹·K⁻² at about 300 °C (Figure 3a). Kumar et al. [32] used a solvent–hydrothermal method to synthesize Sr-filled Sr_yCoSb₃ (y = 0, 0.025, 0.05, 0.075, 0.1) nanoparticles (Figure 3b). The ultraviolet-visible spectral analysis showed that the peak shifted toward the long-wave direction with the increase of Sr filling (Figure 3c), which proved that Sr successfully filled the voids of the CoSb₃ cage structure. The PXRD spectral analysis concluded that the spatial structure of CoSb₃ is bcc structure, and the space group is *Im-3*. It was also found that the spectral peak (013) of the sample after Sr filling was shifted to a high angle (Figure 3d) and a broad high intensity peak appears. Gharlegghi et al. [33] synthesized n-type CoSb₃ materials with nanostructures using a fast hydrothermal method combined with evacuation and sealed heating (Figure 3e). The materials with CoSb₃ as the main phase were synthesized at different hydrothermal temperatures, and the impurities could be effectively removed to obtain single-phase CoSb₃ materials by increasing the hydrothermal temperature. The CoSb₃ material with nanostructure has a very low thermal conductivity at room temperature (Figure 3f).

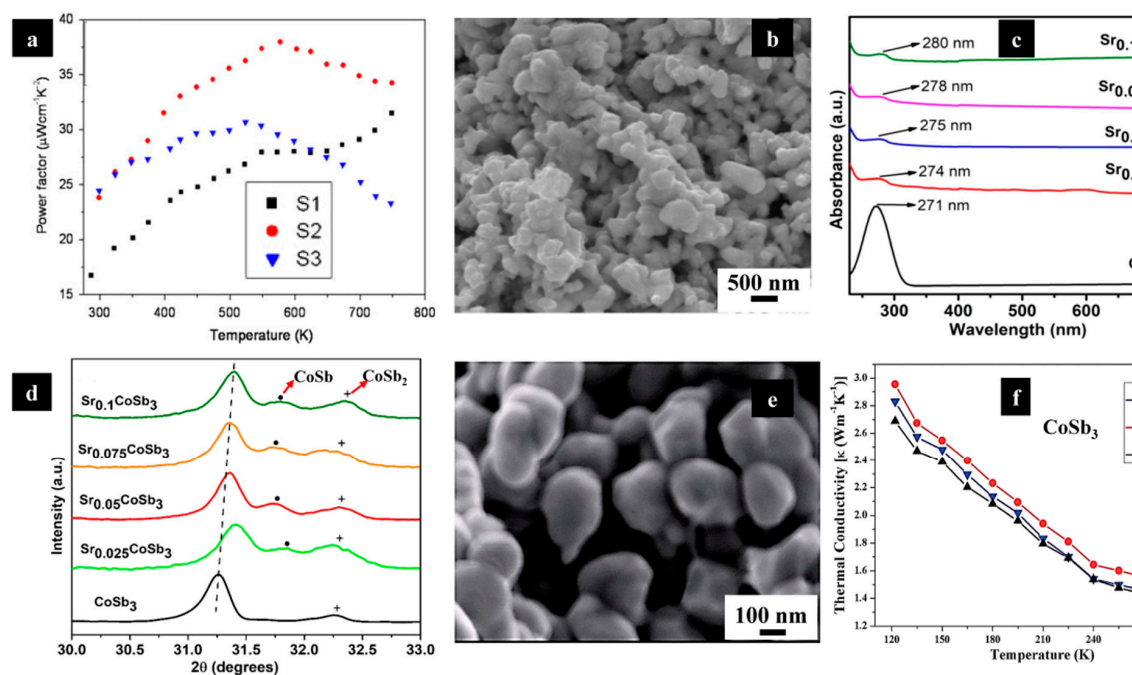


Figure 3. (a) Temperature dependence of power factor for In-filled and Te-doped CoSb_3 samples. S1: $\text{Co}_4\text{Sb}_{11.5}\text{Te}_{0.5}$ sample ($500\text{ }^\circ\text{C} \times 24\text{ h}$), S2: $\text{In}_{0.5}\text{Co}_4\text{Sb}_{11.5}\text{Te}_{0.5}$ sample (long-time annealing); and S3: $\text{In}_{0.5}\text{Co}_4\text{Sb}_{11.5}\text{Te}_{0.5}$ sample (short-time annealing) [31]; (b) FESEM image of $\text{Sr}_{0.05}\text{CoSb}_3$ nanoparticles; (c) UV–visible spectra and (d) XRD patterns of Sr_yCoSb_3 ($y = 0, 0.025, 0.05, 0.075$ and 0.1) samples [32]; (e) FESEM image of CoSb_3 samples prepared by a rapid hydrothermal procedure combined with evacuated-and-encapsulated heating; (f) temperature dependence of thermal conductivity for CoSb_3 samples synthesized at different hydrothermal temperatures ($170, 230$ and $290\text{ }^\circ\text{C}$) [33].

In summary, skutterudite materials with nanostructures can be successfully prepared by the solvothermal method, and the abundant nanostructures can increase the grain boundaries of scattered phonons and significantly reduce the lattice thermal conductivity of the materials [34]. Meanwhile, the quantum confinement effect generated by the low-dimensional nanostructure causes an increase in the density of states near the Fermi surface of the material, which can effectively enhance the Seebeck coefficient. Thus, a synergistic regulation of the electrical and thermal transport properties of thermoelectric materials is achieved, which ultimately improves their ZT values.

2.3. Solid Phase Reaction Method

The solid phase reaction method, also called melt annealing method, is one of the traditional methods for the preparation of skutterudite materials [35–40]. In this method, pure monomers or compounds are weighed, mixed, pressed into shape, vacuum sealed according to the reaction ratio and then subjected to a long solid phase reaction at high temperatures. The method is simple to operate and the temperature is easily controlled. The preparation time of the material is long and the cost is high. Su et al. [40] synthesized single-phase $\text{CoSb}_{2.75}\text{Ge}_{0.25-x}\text{Te}_x$ ($x = 0.125\sim 0.20$) skutterudite compounds using melt quenching, annealing and spark plasma sintering (SPS) methods. The doping of Te and Ge led to the in situ generation of special nanostructures inside the material (about 30 nm) (Figure 4a), which, combined with the strain fluctuations caused by Te and Ge doping, led to a significant suppression of heat transfer phonons inside the material and a significant reduction of thermal conductivity (Figure 4b). In addition, the doping of Te also optimizes the mobility, significantly enhancing the electrical conductivity (Figure 4c) and TE power factor of the material. As a result, the ZT value of the $\text{CoSb}_{2.75}\text{Ge}_{0.05}\text{Te}_{0.20}$ sample can exceed 1.1 at $527\text{ }^\circ\text{C}$, which is higher than the performance of some single-filled n-type skutterudite compounds. In conclusion, the thermoelectric materials prepared by solid

state reaction are compact in structure, uniform in components and stable in performance, making it a good method for the preparation of skutterudite materials.

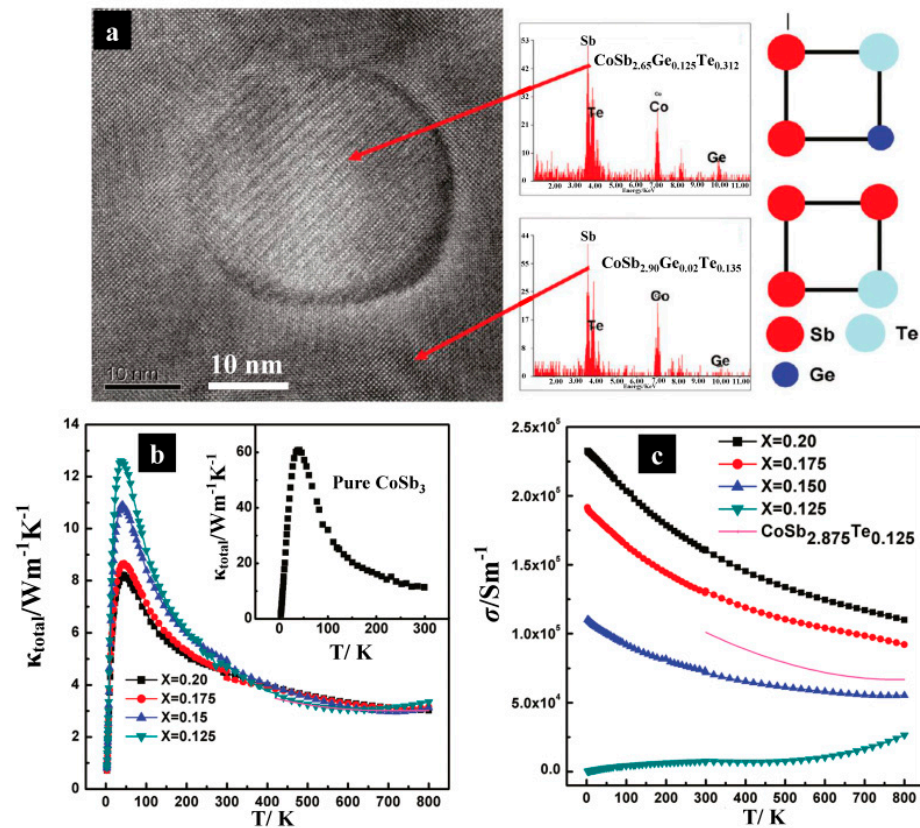


Figure 4. (a) Nanostructure consisting of circular shapes produced in situ inside the material; (b) temperature dependence of thermal conductivity and (c) electrical conductivity for $\text{CoSb}_{2.75}\text{Ge}_{0.25-x}\text{Te}_x$ ($x = 0.125\text{--}0.20$) [40].

2.4. Mechanical Alloying Method

The mechanical alloying method is a preparation technique in which several monolithic powder particles are put into a high-energy planetary ball mill in a specific ratio, after which the powder particles are impressed, squeezed, and ground for a long time to cause the diffusion of atoms among the powder particles to obtain nanoscale alloyed powders [41]. Due to the extremely high purity requirements of the mechanical alloying on the monolithic powder, it is theoretically possible to achieve real interatomic bonding and the formation of homogeneous compounds in a sufficiently long-time state. In fact, the obtained material only reaches or tends to the atomic level in some states, forming compounds of homogeneous composition. This method is also often used to prepare the skutterudite materials [42–46]. Ur et al. [42] synthesized $\text{Fe}_x\text{Co}_{4-x}\text{Sb}_{12}$ ($0 \leq x \leq 2.5$), Fe-doped skutterudite by mechanical alloying using a high-purity monolithic powder as a starting material. It was found that single-phase skutterudite with a nanostructure could be successfully prepared by introducing Fe doping when $x \leq 1.5$; when $x \geq 2$, the material forms a second phase. $x \leq 1.5$ samples have lower lattice thermal conductivity due to the introduction of Fe to increase the nanostructure, which causes strong phonon scattering and thus improves the TE properties. $x = 1.5$ samples have a ZT value reaching 0.3 at 600 K (Figure 5a). Liu et al. [43] used a combination of mechanical alloying and the SPS preparation process to obtain polycrystalline CoSb_3 materials. The grain sizes of the materials obtained at different SPS sintering temperatures (600 °C, 500 °C, 400 °C and 300 °C) were different, as shown in Figure 5(b–e). The grain size increased from 50 to 300 nm when the temperature was increased from 300 °C to 600 °C. It was shown that mechanical alloying

combined with SPS could obtain nanostructured materials with significantly lower thermal conductivity compared to CoSb_3 materials prepared by other methods [45], as shown in Figure 5f. Trivedi et al. [45] used a high-energy ball-milling and SPS sintering technique to successfully fabricate Ni-doped and Dy-filled CoSb_3 material. Although the Seebeck coefficient of the doped material did not change much, Ni replaced the defects caused by Co (Figure 5g) and grain boundary-enhanced phonon scattering, which reduced the thermal conductivity of the lattice. This study also found a significant decrease in resistivity with increasing Ni doping concentration at higher temperatures, leading to an increase in the power factor of the prepared ternary material $\text{Dy}_{0.4}\text{Co}_{3.2}\text{Ni}_{0.8}\text{Sb}_{12}$ and reaching a maximum value of $5.2 \text{ mW}/(\text{m}\cdot\text{K}^2)$ (Figure 5h). Rogl et al. [46] prepared multi-filled n-type skutterudite $(\text{Sr}, \text{Ba}, \text{Yb}, \text{In})_y\text{Co}_4\text{Sb}_{12}$ by high energy ball milling and hot pressing, using a raw material that was doped with a certain percentage of $\text{In}_{0.4}\text{Co}_4\text{Sb}_{12}$ in $(\text{Sr}, \text{Ba}, \text{Yb})_y\text{Co}_4\text{Sb}_{12}$. It was found by analysis that In entered the Sb_{12} dodecahedral voids of the cubic cobaltite regardless of the percentage of doping. At the same time, the total thermal conductivity of the material decreases with increasing In content. As a result, the prepared samples were characterized by small particles, high power factor and low thermal conductivity, and the prepared samples reached a maximum ZT of 1.8 at 550°C (Figure 5i).

In summary, like the solvothermal method, the mechanical alloying method can also prepare high-performance TE materials with abundant nanostructures by high-energy ball milling. The yield of TE materials synthesized by the mechanical alloying method is significantly higher compared to the solvothermal method. For the mass production of TE materials, the mechanical alloying method is significantly better than the solvothermal method.

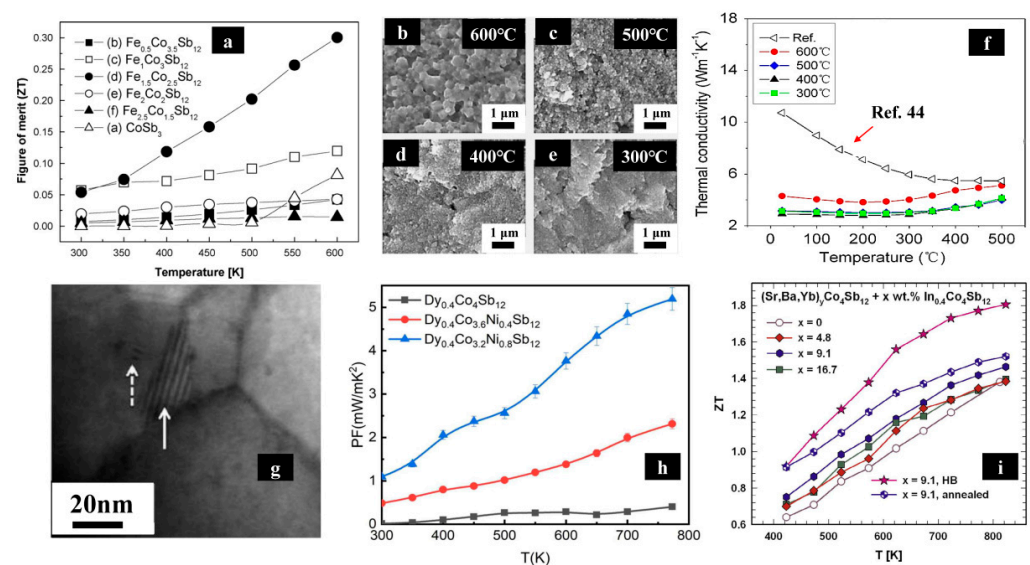


Figure 5. (a) Temperature dependence of ZT values and temperature of $\text{Fe}_x\text{Co}_{4-x}\text{Sb}_{12}$ ($0 \leq x \leq 2.5$) [42]; (b–e) FESEM images of CoSb_3 materials at different sintering temperatures; (f) temperature dependence of thermal conductivity for polycrystalline CoSb_3 materials prepared at different sintering temperatures [43]; (g) HRTEM image of $\text{Dy}_{0.4}\text{Co}_{3.2}\text{Ni}_{0.8}\text{Sb}_{12}$ (dotted arrow points to the defect in the particle and solid arrow points to the Moire fringe); (h) temperature dependent of power factor for Ni doped Dy filled CoSb_3 samples [45]; (i) temperature dependence of ZT values for $(\text{Sr}, \text{Ba}, \text{Yb})_y\text{Co}_4\text{Sb}_{12}$ [46].

3. New Preparation Methods

3.1. Melt Spinning

Melt spinning is one of the new methods for the preparation of TE materials at present [47–52]. This method is performed by weighing and mixing a certain stoichiometric amount of high-purity single elements in a vacuum quartz tube, heating it above

the melting point of the material for a certain time, and then quenching it. Finally, the sample is subjected to melt-spin at a certain speed, after which the finished product can be annealed and sintered to obtain the bulk material. A p-type Ce-filled skutterudite material $\text{Ce}_{0.9}\text{Fe}_3\text{CoSb}_{12}$ was prepared by Jie et al. [49] using both equilibrium (conventional solid phase method) and non-equilibrium (melt-spin) methods. By studying the fracture surface scanning electron microscopy (FESEM) image of the material (Figure 6a), it was found that the fracture direction of the material tends to propagate more along the grain boundaries (which may have good fracture strength), and the grain size (nano size) is much smaller than that prepared by the conventional method. Compared with the $\text{Ce}_{0.9}\text{Fe}_3\text{CoSb}_{12}$ material prepared by the conventional solid-phase reaction, the material prepared by the melt spinning has abundant nano-grain boundaries that can significantly scatter phonons as well as a large number of defects that significantly reduce the thermal conductivity (Figure 6b). At the same time, the quantum-limited domain effect generated by the low-dimensional nanostructure causes an increase in the density of states near the Fermi surface of the $\text{Ce}_{0.9}\text{Fe}_3\text{CoSb}_{12}$ material, which can effectively increase the Seebeck coefficient and thus the power factor of the material (Figure 6c).

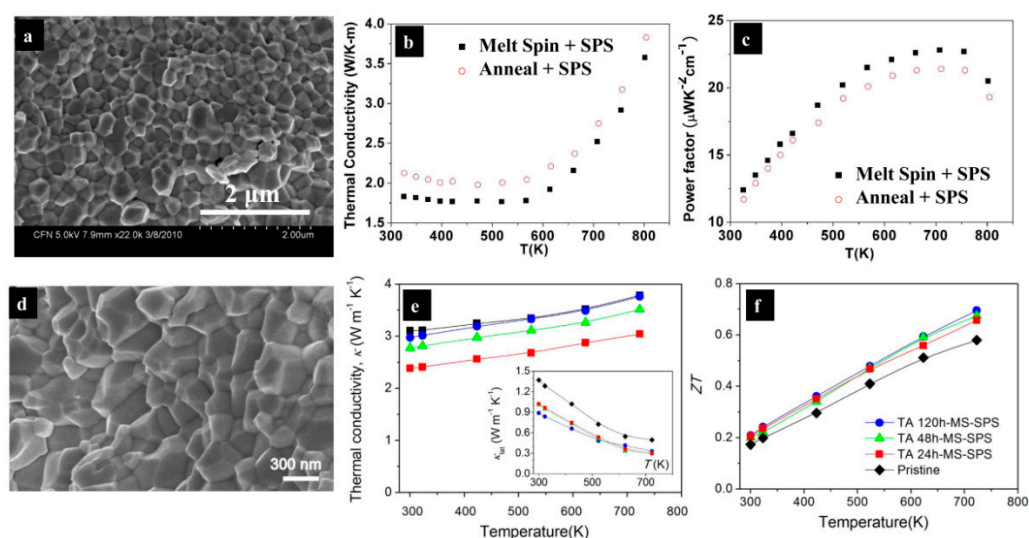


Figure 6. (a) SEM image of fracture surface of $\text{Ce}_{0.9}\text{Fe}_3\text{CoSb}_{12}$ material; temperature dependence of (b) power factor and (c) thermal conductivity for the $\text{Ce}_{0.9}\text{Fe}_3\text{CoSb}_{12}$ material [49]; (d) SEM image of $\text{Yb}_{0.9}\text{Fe}_3\text{CoSb}_{12}$ sample; temperature dependence of (e) thermal conductivity and (f) ZT values for $\text{Yb}_{0.9}\text{Fe}_3\text{CoSb}_{12}$ material prepared under different preparation conditions. The inset shows the temperature dependence of lattice thermal conductivity [50].

Son et al. [50] prepared single-phase polycrystalline $\text{Yb}_{0.9}\text{Fe}_3\text{CoSb}_{12}$ TE materials with high-density grain boundaries and nanostructures by means of melt spinning and spark plasma sintering (MS–SPS). This high density of grain boundaries and nanostructure (Figure 6d) has a strong scattering effect on phonons, resulting in a material with a low thermal conductivity (Figure 6e). The $\text{Yb}_{0.9}\text{Fe}_3\text{CoSb}_{12}$ sample prepared by the MS–SPS process after annealing at 120 h (TA 120h–MS–SPS) had the highest ZT value of 0.7 (Figure 6f).

Like the solvothermal and mechanical alloying methods, the melt-spinning method can prepare high-performance TE materials with abundant nanostructures. Moreover, the preparation time of the melt-spinning method is shorter than that of the mechanical alloying method, which can prepare TE materials more rapidly and is more suitable for mass production.

3.2. High-Temperature and High-Pressure Method

The high-temperature and high-pressure (HTHP) method is one of the effective methods to prepare high-performance skutterudites [53–58]. Generally, the experimental raw

materials are weighed in a fixed proportion, fully ground under Ar atmosphere (to prevent the material from being oxidized), and later placed in a vessel for sintering at a certain temperature and pressure. This method is convenient for controlling the external temperature and pressure conditions, while it can greatly reduce the experimental time and has important practical significance in large-scale production. Han et al. [55] prepared Te-doped filled skutterudites under different pressure conditions using a high temperature and high-pressure method and investigated the synergistic relationship between Te doping and pressure regulation. It was found that Te doping could effectively optimize the electrical transport properties of the samples, while some defects appeared in the crystals at high pressure (Figure 7a). This further reduced the lattice thermal conductivity of the materials, and the lattice thermal conductivity of the $\text{In}_{0.05}\text{Ba}_{0.15}\text{Co}_4\text{Sb}_{11.5}\text{Te}_{0.5}$ samples prepared at 2.0 GPa was only $1.02 \text{ W}\cdot\text{m}^{-1}\cdot\text{K}^{-1}$ with a maximum ZT value of 1.23 (Figure 7b). Kong et al. [56] synthesized Ni-substituted Ba-filled skutterudite $\text{Ba}_{0.3}\text{Ni}_{0.15}\text{Co}_{3.85}\text{Sb}_{12}$ using the high-temperature and high-pressure method. The electrical transport properties of the material were obviously optimized by the pressure regulation. The thermal transport properties were significantly improved by adding various grain boundaries and generating various lattice distortions (Figure 7c). Figure 7(d–g) shows the FESEM images of the material at 2–3.5 GPa with a vortex-like structure and a smaller average grain size at higher pressures. The synthesis time for this experiment was controlled at 30 min. The ZT value of the sample prepared at a pressure of 3.0 GPa reached 0.91 (Figure 7h). Jiang et al. [57] synthesized Te and Sn co-doped skutterudite $\text{CoSb}_{2.75}\text{Te}_{0.2}\text{Sn}_{0.05}$ materials using the high-temperature and high-pressure method. This method can shorten the fabrication process to 1 h, which saves a lot of time compared to other traditional methods. Due to the enhanced phonon scattering from point defects caused by the high-temperature and high-pressure method, the thermal conductivity of the material decreased significantly with increasing pressure. The 3 GPa sample prepared at high pressure reached a maximum ZT value of 1.17 (Figure 7i).

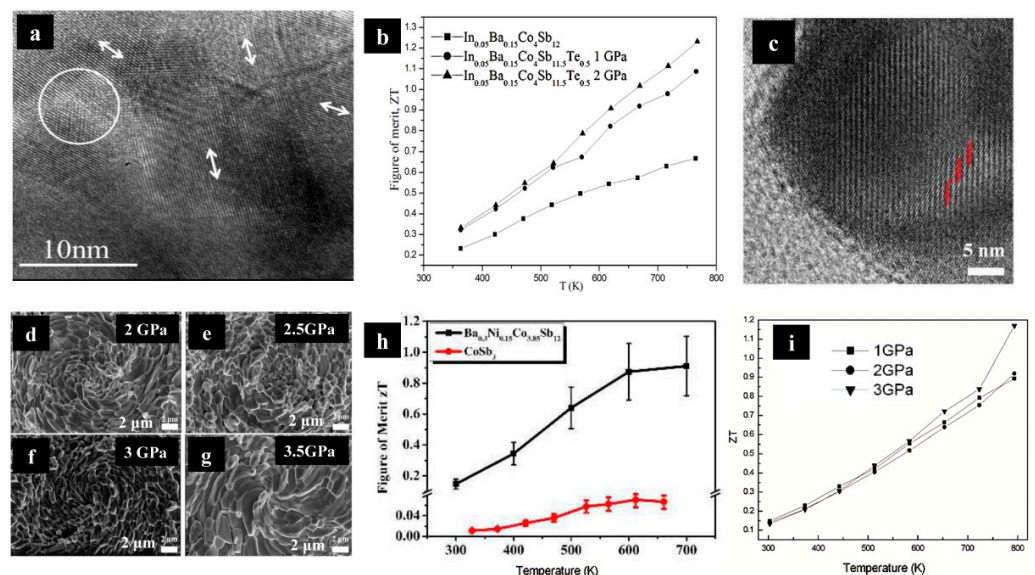


Figure 7. (a) HRTEM image of $\text{In}_{0.05}\text{Ba}_{0.15}\text{Co}_4\text{Sb}_{11.5}\text{Te}_{0.5}$ material; (b) temperature dependence of ZT values for $\text{In}_{0.05}\text{Ba}_{0.15}\text{Co}_4\text{Sb}_{12}$ and $\text{In}_{0.05}\text{Ba}_{0.15}\text{Co}_4\text{Sb}_{11.5}\text{Te}_{0.5}$ samples [55]; (c) HRTEM image of $\text{Ba}_{0.3}\text{Ni}_{0.15}\text{Co}_{3.85}\text{Sb}_{12}$ material; (d–g) FESEM images of $\text{Ba}_{0.3}\text{Ni}_{0.15}\text{Co}_{3.85}\text{Sb}_{12}$ prepared under different pressures; (h) temperature dependence of ZT values for CoSb_3 and $\text{Ba}_{0.3}\text{Ni}_{0.15}\text{Co}_{3.85}\text{Sb}_{12}$ samples at 3 GPa [56]; (i) Temperature dependence of ZT values of $\text{CoSb}_{2.75}\text{Te}_{0.2}\text{Sn}_{0.05}$ sample prepared under different pressure conditions [57].

These findings indicate that the microstructure of the skutterudite materials prepared under certain high-temperature and high-pressure conditions changes significantly, and

some defects that can scatter phonons significantly appear, while the carrier transport is not affected. Thus, the TE properties of the prepared materials can be significantly improved. At the same time, the high-temperature and high-pressure preparation time will be greatly reduced compared to the conventional solid phase reaction method.

3.3. Pulsed Laser Deposition

Pulsed laser deposition (PLD), also known as pulsed laser ablation (PLA), is the use of laser light to bombard a target material so that the bombarded plasma is deposited on a specific substrate to form a thin film. At present, with the continuous development of laser technology, pulsed laser technology is gradually being applied in many material preparation fields [59]. In recent years, pulsed laser deposition has also been applied to the preparation of skutterudite TE films [60–62]. This technique has the advantages of a relatively short preparation time, homogeneous film material composition, and no special requirements for the target type. Sarath et al. [60] prepared In and Yb doped CoSb₃ thin films using pulsed laser deposition. During the preparation, the process window for the growth of single-phase skutterudite thin films was very narrow. It was found that the information and the increase in surface roughness of CoSb₃ after heating in an argon environment may lead to irreversible changes in film resistivity and Seebeck coefficient at 207 °C. The highest power factor of 0.68 W·m⁻¹·K⁻¹ could be obtained for this film at 427 °C (Figure 8a), which is five times lower compared to most of the blocks, probably due to the high resistivity of the film material. Jelinek et al. [61] prepared Yb-filled CoSb₃ films using pulsed laser deposition. The films were found to be smoother when the distance from the target material to the substrate was increased, and the conductivity of the films with higher crystallinity of the target material was found to be better. Nanocrystalline films of 50–80 nm were prepared at 270 °C (Figure 8b). The ZT value at room temperature was measured to be about 0.04. The thermal conductivity was calculated for different types and thicknesses of films to be only 0.4–1.3 WK⁻¹m⁻¹. Masarrat et al. [62] deposited single-phase CoSb₃ films on a substrate of Si using CoSb₃ as a polycrystalline target using a pulsed laser deposition method (Figure 8(c1,c2)). The samples with added Fe have low resistivity and high Seebeck coefficient (Figure 8d) leading to a high power factor, so the TE properties of CoSb₃ thin film materials can be significantly enhanced by adjusting the Fe content.

3.4. Magnetron Sputtering

Magnetron sputtering is one of the types of physical vapor deposition (PVD). With the advantages of magnetron sputtering coming to the fore, it has gradually gained wide application [63]. The specific principle is that when the accelerated electrons hit the argon atoms, the resulting argon ions then collide with the target material, causing the bombarded target atoms to be deposited on the substrate to form a thin film. This technique has the characteristics of fast low temperature, large deposition rate, and can be made into a large area of thin film. In recent years, this technique has also been applied to the preparation of skutterudite TE films [64–66]. Fan et al. [64] used magnetron sputtering to grow Ag-doped CoSb₃ films directly on heated substrates (Figure 9a). It was found that the doped films had a single-phase CoSb₃ crystal structure and good crystallinity, and the CoSb₃ films with high electrical transport properties could be obtained with the appropriate amount of doping. The films had a maximum power factor of 2.97×10^{-4} W·m⁻¹·K⁻² at 0.3% Ag doping (Figure 9b). Zheng et al. [65] prepared CoSb₃ films with excess Co and Sb using radio frequency and direct magnetron sputtering. It was shown that the films containing excess Co had n-type conduction behavior and the films containing excess Sb had p-type conduction behavior. The right ratio of Co and Sb can effectively improve the electrical conductivity of the films, and the excess of Sb has a larger carrier mobility (Figure 9c), which results in better electrical transport properties (Figure 9d), and the calculated material power factor reaches 6.9×10^{-4} W·m⁻¹·K⁻², which is 10 times higher than that of binary CoSb₃ films. Therefore, the authors also speculated that Sb might be an important element

to improve the performance of TE materials. Li et al. [66] prepared Ti and In double-doped CoSb₃ TE films by magnetron sputtering. By optimizing the sputtering time of CoSb₃, Ti and In doped CoSb₃ TE films S4 with optimal electrical transport properties were obtained. The experimental conditions for the S4 film samples were 30 min for CoSb₃ sputtering, 60 s for Ti sputtering and 30 s for In sputtering.

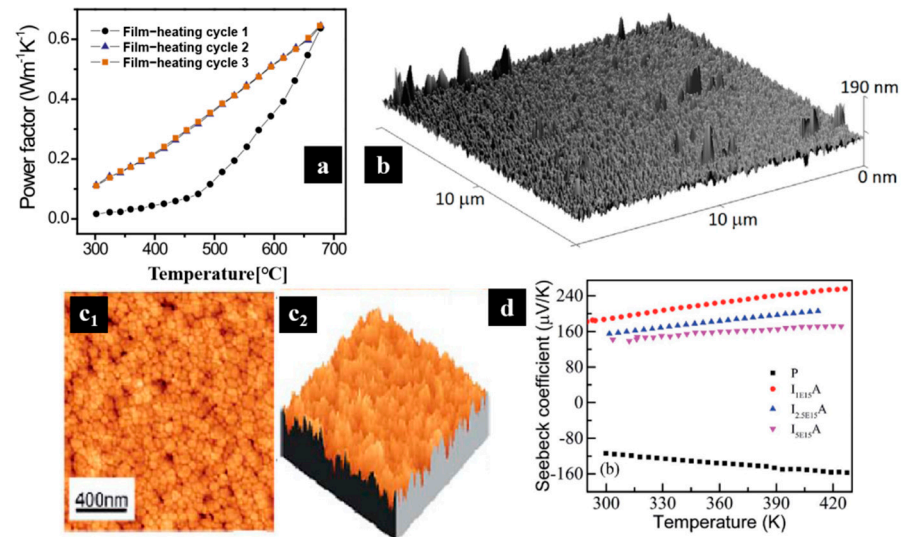


Figure 8. (a) Temperature dependence of power factor for In and Yb doped CoSb₃ films [60]; (b) AFM image of Yb-filled CoSb₃ film material surface [61]; (c₁,c₂) 2D and 3D AFM images of single-phase CoSb₃ film; (d) temperature dependence of Seebeck coefficient for single-phase CoSb₃ and Fe-doped CoSb₃ film [62]. P is untreated single-phase CoSb₃ film. I_{1E15}A, I_{2.5E15}A and I_{5E15}A are CoSb₃ films annealed rapidly and added with 1×10^{15} , 2.5×10^{15} or 5×10^{15} iron ions per square centimeter, respectively.

3.5. Molecular Beam Epitaxy (MBE)

MBE is a novel method for the epitaxial preparation of thin film materials and has also been used in recent years for the preparation of skutterudite TE thin film materials [67–71]. MBE is a novel process for coating on substrates under ultra-high vacuum. The advantages of this preparation method are: (1) the thickness of the film can be precisely controlled at a slower growth rate; (2) the preparation method is a physical process without considering intermediate chemical processes, which can interrupt the progress of the experiment at any time; and (3) the substrate temperature of this method does not need to be too high, which reduces various adverse effects caused by thermal expansion, etc. Daniel et al. [69] deposited CoSb₃ thin films with a thickness of 30 nm at different substrate temperatures using the MBE method. It was found that the deposition method and the temperature of the substrate used for the deposition process had a significant effect on the grain size of the CoSb₃ films, and the higher the temperature, the smaller the grain size (Figure 10a). After deposition at room temperature, annealing is required to crystallize them, and they can crystallize into phases quickly when deposited at high temperatures. The annealed film has a very smooth surface, less roughness, and possesses a larger single-phase component. In addition, the smaller grain size of the films prepared at higher substrate temperatures allows for lower thermal conductivity. Makogon et al. [71] investigated the phase composition and crystal structure of CoSb_x ($1.82 \leq x \leq 4.16$) nanofilms grown on oxidized single-crystal silicon substrates using MBE at 200 °C. It was found that increasing the percentage of Sb in CoSb_x produced different substances (Figure 10b): when the content of Sb was 64.5%, the films consisted of CoSb₂; when the content of Sb was 64.5% to 75%, the films consisted of CoSb₂ and CoSb₃; when the content of Sb was 75%, the films consisted of CoSb₃; when the content of Sb exceeded 75%, the films consisted of CoSb₃ and Sb. Figure 10c presents

the resistivity of the skutterudite films with different Sb contents. It can be seen that the variation of Sb content has a large effect on the resistivity of the prepared thin film material.

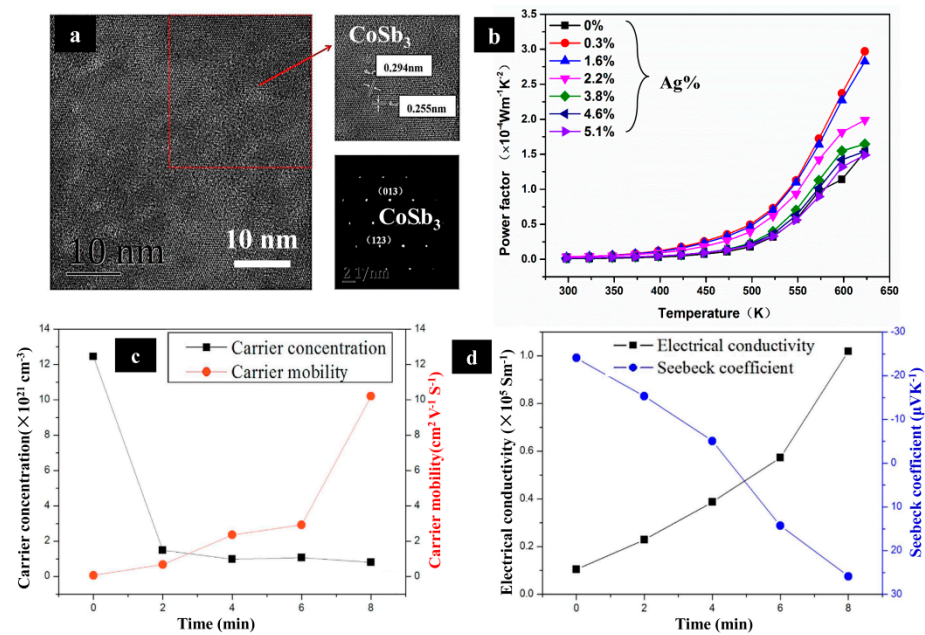


Figure 9. (a) HRTEM image of the Ag-doped sample; (b) temperature dependence of power factor for Ag-doped CoSb_3 thin film samples [64]; (c) carrier concentration and Hall mobility of CoSb_3 films with Sb excess with deposition time; (d) Seebeck coefficient and electrical conductivity of CoSb_3 films with Sb excess with deposition time [65].

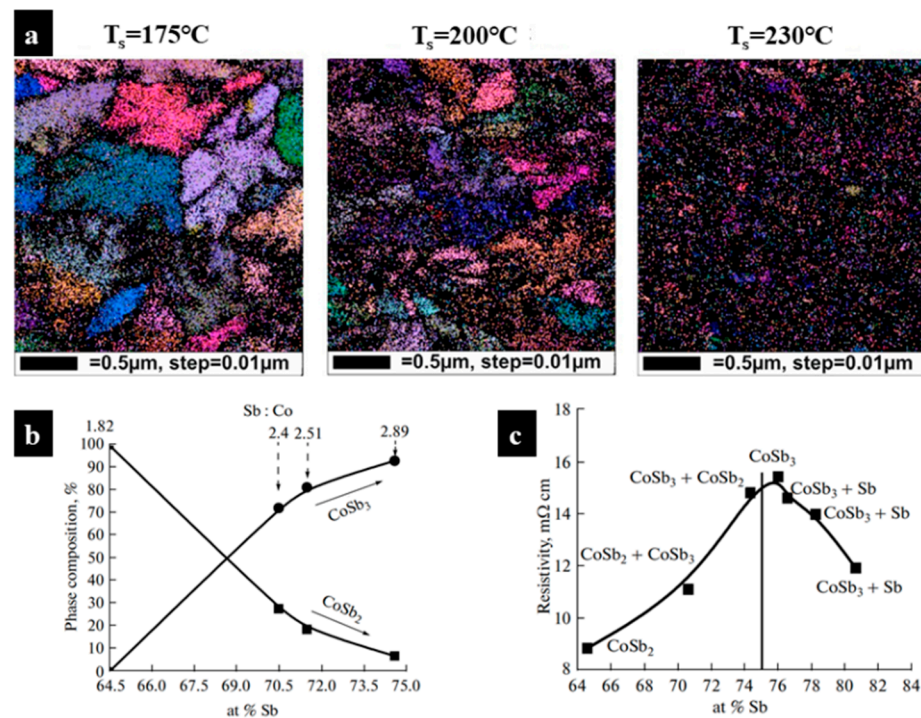


Figure 10. (a) EBSD analysis of CoSb_3 films at different substrate temperatures [69]; (b) effect of Sb content on phase composition of grown CoSb_x ($1.82 \leq x \leq 2.89$) films; (c) Sb content dependence of resistivity for CoSb_x films [71].

Three novel preparation methods, namely, pulsed laser deposition, magnetron sputtering and molecular beam epitaxy, can be used to obtain low-dimensional skutterudite

thin film materials. It is expected to provide technical support for the preparation of miniaturized and efficient TE devices.

3.6. Self-Spreading High-Temperature Synthetic (SHS)

The self-spreading high-temperature synthetic process is also called combustion synthesis technology (SHS) [72–74]. This technology uses external energy to initiate chemical reactions. Then, the exothermic reaction is used to initiate new chemical reactions. Thus, the chemical reaction will spread to the whole reactor. Finally, the target product can be obtained. Su et al. [75] proposed for the first time the use of SHS for the rapid preparation of TE materials. This article also reported a high-performance Cu_2Se TE material. Because this technology has the characteristics of high purity of products, low energy consumption, simple equipment and short reaction time, TE researchers have rapidly prepared high-performance TE materials of different systems through SHS [27,76–78]. Liang et al. [27] applied SHS to the synthesis of CoSb_3 TE materials for the first time. In this experiment, the single-phase CoSb_3 material was quickly synthesized by igniting the powder of Co and Sb (Figure 11a) using the characteristics of heat released by chemical reaction. Then, $\text{CoSb}_{3-x}\text{Te}_x$ bulk materials were prepared by plasma-activated sintering (PAS). The bulk materials prepared by SHS-PAS have rich nanostructures (Figure 11b). Combined with Te-doping to control the carrier concentration of the material, the electrical conductivity of the material is improved. As a result, the maximum ZT value of this sample at 547 °C is 0.98 (Figure 11c), which is the $\text{CoSb}_{2.85}\text{Te}_{0.15}$ sample prepared by SHS-PAS. This method reduces the traditional preparation time to about 20 min, which provides a new idea for the large-scale industrial application of TE materials in the future.

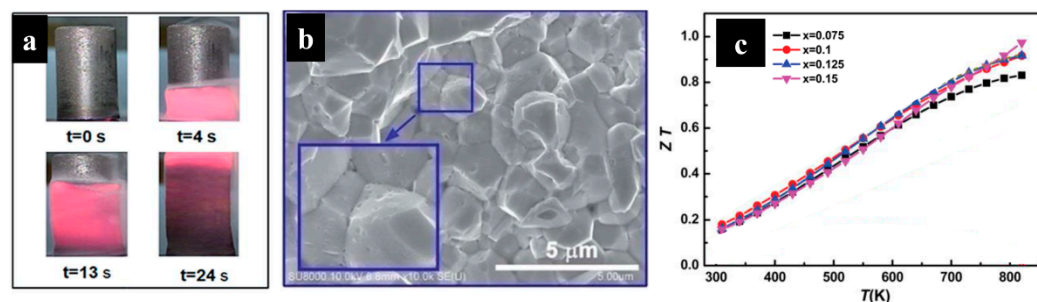


Figure 11. (a) Different stages of the SHS process; (b) the FESEM image of the bulk $\text{CoSb}_{3-x}\text{Te}_x$ compound after SHS-PAS processing; (c) the dimensionless figure of merit ZT of $\text{CoSb}_{3-x}\text{Te}_x$ compound after SHS-PAS processing [27].

3.7. Microwave Sintering

At present, $300\sim 3 \times 10^5$ MHz is generally defined as the microwave frequency band. Its wavelength is $1\sim 1 \times 10^3$ mm. In practice, the microwave frequency band used in microwave sintering is 2.45×10^3 MHz. Because microwaves can be absorbed by materials, it changes from electromagnetic energy to thermal energy in the material, which makes the material temperature rise rapidly and realizes the purpose of sintering. Compared with traditional sintering, microwave sintering has the characteristics of short sintering time, selective sintering and energy saving. Thus, the sintering process has also been used in the preparation of TE materials in recent years [79–84]. Biswas et al. [79] used a microwave synthesis device (Figure 12a) to synthesize $\text{In}_{0.2}\text{Co}_4\text{Sb}_{12}$ skutterudite powder in a short time (2 min), which is much shorter than the traditional preparation method (3 days). After sintering, the ZT value of the powder sample synthesized by microwave is equivalent to that of the bulk sample obtained by the traditional preparation method (Figure 12b). Lei et al. [82] also prepared a series of Te-doped skutterudite $\text{CoSb}_{3-x}\text{Te}_x$ ($x = 0, 0.05, 0.10, 0.20, 0.30$) by microwave synthesis combined with spark plasma sintering. At the same time, they also studied the effect of Te content on the TE properties of the samples. The $\text{CoSb}_{2.95}\text{Te}_{0.05}$ sample (Figure 12c) synthesized by microwave has a large

number of dislocations and strongly scattered phonons at grain boundaries, which makes it have the lowest lattice thermal conductivity ($1.04 \text{ W}\cdot\text{m}^{-1}\cdot\text{K}^{-1}$). Because Te doping regulates the carrier concentration of the sample, the electrical transport performance is also significantly improved. Therefore, the highest ZT value of 1.06 is obtained for the $\text{CoSb}_{2.95}\text{Te}_{0.05}$ sample at 773 K (Figure 12d).

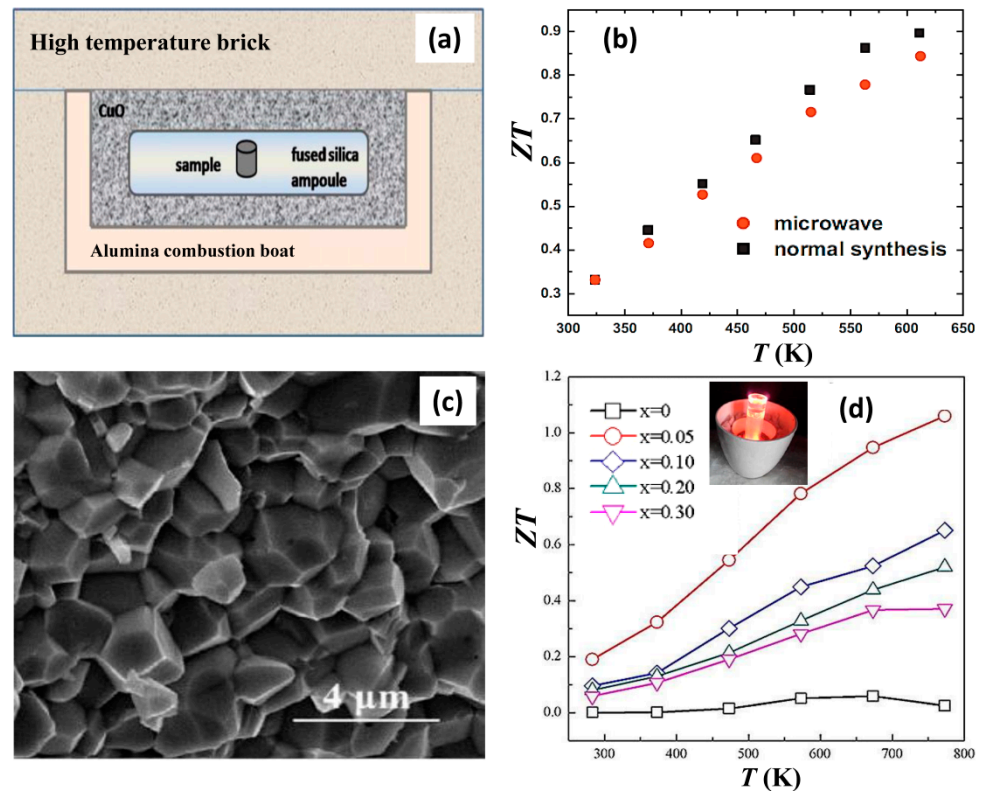


Figure 12. (a) Schematic of the setup used for the microwave synthesis of $\text{In}_{0.2}\text{Co}_4\text{Sb}_{12}$ material; (b) temperature dependence of the ZT of samples prepared with the normal method and microwave method [79]; (c) FESEM image of cross-section of $\text{CoSb}_{2.95}\text{Te}_{0.05}$ sample prepared with the microwave method; (d) temperature dependence of ZT of $\text{CoSb}_{3-x}\text{Te}_x$ samples [82].

Compared with the traditional preparation method, this preparation technology has the advantages of short time and high efficiency. Therefore, it is expected to be a more energy-saving and economic way to prepare high-performance TE materials.

3.8. High Pressure Torsion (HPT)

Severe plastic deformation (SPD) of materials can be formed via high-pressure torsion (HPT). The ultra-fine grains in the sub-micrometer or nanometer range can be obtained by SPD via HPT [85]. At the same time, a large number of dislocations will be produced in the material. Due to the huge changes in the grain size and dislocation density of the materials, these changes will significantly improve the performance of the TE materials [86]. It enables the production of samples in large quantities (50 g) by this advanced preparation technology, and is therefore usable for industrial production [87–89]. A high ZT value of p- and n-type skutterudites can be obtained through this advanced preparation technology [87,88]. Rogl et al. [87] prepared p-type skutterudite $\text{DD}_{0.7}\text{Fe}_{2.7}\text{Co}_{1.3}\text{Sb}_{11.7}\{\text{Ge}/\text{Sn}\}_{0.3}$ using the reaction–annealing–melting technique. Because the $\text{DD}_{0.7}\text{Fe}_{2.7}\text{Co}_{1.3}\text{Sb}_{11.8}\text{Sn}_{0.2}$ sample has low thermal conductivity, the highest ZT value of this p-type skutterudite reaches 1.3. The authors claim that this is the highest ZT value of p-type skutterudite reported. After SPD via HPT, although the resistivity of the material increases, it is compensated by the significantly reduced thermal conductivity due to the additional introduction of defects.

Therefore, the highest ZT value of this sample increases to 1.45 at 850 K. Rogl et al. [88] also prepared n-type skutterudite $\text{Sr}_{0.07}\text{Ba}_{0.07}\text{Yb}_{0.07}\text{Co}_4\text{Sb}_{12}$ by HPT. It was found that the thermal conductivity decreased significantly after HPT due to the presence of lattice defects like dislocations (Figure 13a) and vacancies induced by the SPD process. The lattice thermal conductivity almost reached the minimum value calculated theoretically. The highest ZT value of the sample increased from 1.4 to 1.8 (Figure 13b).

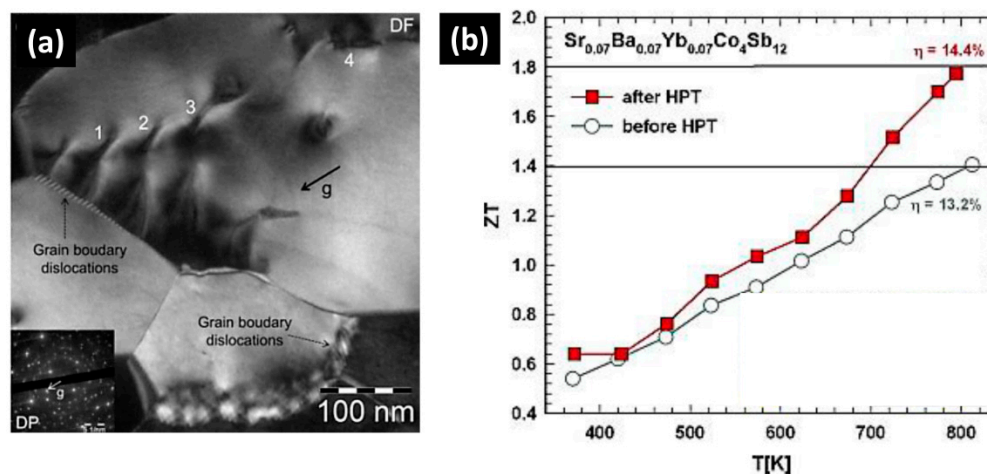


Figure 13. (a) Energy-filtered high-magnification dark-field TEM images of $\text{Sr}_{0.07}\text{Ba}_{0.07}\text{Yb}_{0.07}\text{Co}_4\text{Sb}_{12}$ (cross section); Positions 1, 2, 3 and 4 represent some dislocation structures. (b) temperature-dependent ZT of $\text{Sr}_{0.07}\text{Ba}_{0.07}\text{Yb}_{0.07}\text{Co}_4\text{Sb}_{12}$ sample before HPT and after HPT [88]. Insert in (a): energy-filtered selected area diffraction pattern.

Compared with other preparation methods, as shown in Table 1, the skutterudite materials prepared by this HPT technology have higher ZT values. The preparation time is not long (about 15 min), the grain size of the prepared skutterudite by this technology is also at the nanometer level. In addition, it enables the production of samples in large quantities (50 g) using this technology, and is therefore usable for industrial production. Therefore, HPT technology is one of the very important methods to prepare high-performance TE materials.

Table 1. Preparation methods, preparation time, grain size and ZT values of several typical skutterudite materials.

Traditional Preparation Method	Skutterudites	Preparation Time	ZT	Grain Size	References
Melt growth	CoSb_3	840 h	—	—	[28]
	CoSb_3	40 h	0.47	20–200 μm	[30]
Solvothermal	$\text{In}_x\text{Co}_4\text{Sb}_{12}$	24 h	0.92	1–5 μm	[31]
	Sr_yCoSb_3	24 h	—	50–120 nm	[32]
	CoSb_3	12 h	0.016 (RT)	50–100 nm	[33]
Solid phase reaction	$\text{BaInFe}_{3.7}\text{Co}_{0.3}\text{Sb}_{12+m}$	192 h	0.63	2–10 μm	[35]
	$\text{Se}_y\text{Co}_{4-x}\text{Pd}_x\text{Sb}_{12-2y}\text{Se}_{2y}$	60 h	0.9	1–4 μm	[38]
	$\text{SyPd}_x\text{Co}_{4-x}\text{Sb}_{12}$	72 h	0.85	1–3 μm	[39]
	$\text{CoSb}_{2.75}\text{Ge}_{0.25-x}\text{Te}_x$	198 h	1.1	5–40 nm	[40]
MA	$\text{Fe}_x\text{Co}_{4-x}\text{Sb}_{12}$	100 h	0.3	20–80 nm	[42]
	$\text{Dy}_{0.4}\text{Co}_{3.2}\text{Ni}_{0.8}\text{Sb}_{12}$	10 h	1.4	40–200 nm	[45]

Table 1. Cont.

Advanced Preparation Method	Component	Time	ZT	Grain Size	References
MS	$\text{Ce}_{0.9}\text{Fe}_3\text{CoSb}_{12}$	30 h	0.7	1–4 μm	[49]
	$\text{Yb}_{0.9}\text{Fe}_3\text{CoSb}_{12}$	12 h	0.7	100–300 nm	[50]
	$\text{Yb}_x\text{Ba}_y\text{Co}_4\text{Sb}_{12}$	30 min	1.1	—	[52]
HTHP	$\text{In}_{0.05}\text{Ba}_{0.15}\text{Co}_4\text{Sb}_{11.5}\text{Te}_{0.5}$	—	1.23	1–3 μm	[55]
	$\text{Ba}_{0.3}\text{Ni}_{0.15}\text{Co}_{3.85}\text{Sb}_{12}$	25 min	0.91	—	[56]
	$\text{CoSb}_{2.75}\text{Te}_{0.20}\text{Sn}_{0.05}$	30 min	1.17	—	[57]
Pulsed Laser Deposition	$\text{In}_{0.2}\text{Yb}_{0.2}\text{Co}_4\text{Sb}_{12}$	20 ns	—	90–110 nm	[60]
	$\text{Yb}_{0.19}\text{Co}_4\text{Sb}_{12}$	20 ns	0.05 (RT)	50–80 nm	[61]
	CoSb_3	20 ns	—	50–100 nm	[62]
Magnetron sputtering	CoSb_3 (Ag sputter)	15 min	2.97×10^{-4}	—	[63]
	CoSb_3 (Co-excess or Sb-excess)	30 min	6.9×10^{-4}	—	[65]
	CoSb_3 (In and Ti sputter)	1–30 min	2.32×10^{-4}	—	[66]
MBE	CoSb_y	10 min	—	50–150 nm	[69]
	$\text{Yb}_z(\text{CoSb}_3)_4$	1–3 h	>1	—	[70]
	CoSb_x	—	—	30 nm	[71]
SHS	$\text{CoSb}_{2.85}\text{Te}_{0.15}$	10–20 min (SHS-PAS)	0.98	1–2 μm	[27]
	$\text{Co}_4\text{Sb}_{10.8}\text{Te}_{0.6}\text{Se}_{0.6}$	10–20 min (SHS-PPS)	1.1	—	[78]
Microwave sintering	$\text{In}_{0.2}\text{Co}_4\text{Sb}_{12}$	4 min	0.9	—	[79]
	$\text{Co}_4\text{Sb}_{11.9-x}\text{Te}_x\text{Se}_{0.1}$	5 min	0.81	1–6 μm	[81]
	$\text{CoSb}_{3-x}\text{Te}_x$	5 min	1.06	2–5 μm	[82]
	$\text{Ti}_x\text{Co}_4\text{Sb}_{11.5}\text{Te}_{0.5}$	5 min	0.6	1–4 μm	[84]
HPT-SPD	$\text{DD}_{0.7}\text{Fe}_{2.7}\text{Co}_{1.3}\text{Sb}_{11.7}\text{Ge}_{0.1}$	~15 min	>1	15–300 nm	[87]
	$\text{DD}_{0.7}\text{Fe}_{2.7}\text{Co}_{1.3}\text{Sb}_{11.8}\text{Sn}_{0.2}$	~15 min	1.4	15–300 nm	[87]
	$\text{Sr}_{0.07}\text{Ba}_{0.07}\text{Yb}_{0.07}\text{Co}_4\text{Sb}_{12}$	~15 min	1.8	5–250 nm	[88]

4. Conclusions

Skutterudite is a kind of TE material with excellent performance in the middle temperature region, which is expected to have a good application and development prospects in the field of power generation. Due to the special icosahedral cage structure, there are many ways to improve the ZT value of skutterudite material. In order to obtain skutterudite with excellent properties, it is very important to select appropriate preparation methods. This review systematically summarized some traditional and advanced preparation methods of skutterudites in recent years, and the principles of these preparation methods were briefly introduced. The traditional preparation methods of TE materials (such as the solid-state reaction method) are time-consuming and use large amounts of energy, but the prepared materials have high density, are of uniform composition, and have good mechanical properties and stable TE properties. The new preparation method has a shorter preparation time, lower energy consumption and higher properties. The rapidly prepared TE materials usually have different types of defect structures (such as dislocation, pores, superlattice and nano-grain boundaries). These defects help to scatter multi-scale phonons and significantly

reduce the thermal conductivity of the material. Therefore, TE materials can have high TE properties. The approach is relatively poor in terms of densification and mechanical properties compared with traditional preparation methods. Therefore, there are still some problems in the preparation process of TE materials, which need to be further studied.

- (1) We need to further understand the principles of some preparation methods of TE materials and theoretically understand the reaction mechanism of the preparation process, thus providing an important theoretical basis for further optimization of the preparation process;
- (2) We need to further optimize the existing advanced preparation process, such as process parameters and process flow;
- (3) The key to the large-scale production of TE materials is to further explore novel preparation processes. This new preparation process has the advanced characteristics of being less time- and energy-consuming and being more environment-friendly. The prepared TE materials have high density, are of uniform composition and provide stable performance.

The existing traditional and new preparation processes can produce skutterudite materials with good properties. Optimizing the existing preparation process and exploring new preparation processes are the key to making further improvements to the properties of skutterudites. At present, the n-type skutterudite materials prepared by the existing preparation process have higher TE properties, while the p-type skutterudites have lower TE properties. Therefore, it is particularly important to further explore new energy-saving, low-cost, green and sustainable technologies and processes to rapidly prepare high-performance p-type skutterudite materials. It also provides technical support for the large-scale application of TE materials.

Author Contributions: Conceptualization and writing—original draft preparation, C.Z. and M.W.; writing—review and supervision, Z.L. All authors have read and agreed to the published version of the manuscript.

Funding: This study was supported by the National Natural Science Foundation of China under grant no. 51872006, the Excellent Youth Project of the Natural Science Foundation of Anhui Province of China under grant no. 2208085Y17, and the National Undergraduate Training Programs for Innovation and Entrepreneurship under grant no. S202110360181.

Institutional Review Board Statement: Not applicable.

Informed Consent Statement: Not applicable.

Data Availability Statement: Data sharing is not applicable to this review as no datasheets were generated or analyzed during the current study.

Acknowledgments: The authors thank the National Undergraduate Training Programs for Innovation and Entrepreneurship (No. S202110360181) for its support to this work.

Conflicts of Interest: The authors declare no conflict of interest.

References

1. Wise, M.; Calvin, K.; Thomson, A.; Clarke, L.; Bond-Lamberty, B.; Sands, R.; Smith, S.J.; Janetos, A.; Edmonds, J. Implications of limiting CO₂ concentrations for land use and energy. *Science* **2009**, *324*, 1183–1186. [[CrossRef](#)]
2. Denilson, B.E.S. An energy and exergy analysis of a high-efficiency engine trigeneration system for a hospital: A case study methodology based on annual energy demand profiles. *Energy Build.* **2014**, *76*, 185–198.
3. Ioffe, A.F.; Stil'bans, L.S.; Iordanishvili, E.K.; Stavitskaya, T.S.; Gelbtuch, A.; Vineyard, G. Semiconductor Thermoelements and Thermoelectric Cooling. *Phys. Today* **1959**, *12*, 42. [[CrossRef](#)]
4. Zhang, Z.W.; Wang, X.Y.; Liu, Y.J.; Cao, F.; Zhao, L.D.; Zhang, Q. Development on thermoelectric materials. *J. Chin. Ceram. Soc.* **2018**, *46*, 288–305.
5. Qin, D.; Cui, B.; Yin, L.; Zhao, X.; Zhang, Q.; Cao, J.; Cai, W.; Sui, J. Tin Acceptor Doping Enhanced Thermoelectric Performance of n-Type Yb Single-Filled Skutterudites via Reduced Electronic Thermal Conductivity. *ACS Appl. Mater. Interfaces* **2019**, *11*, 25133–25139. [[CrossRef](#)] [[PubMed](#)]

6. Xu, W.J.; Zhang, Z.W.; Liu, C.Y.; Gao, J.; Ye, Z.Y.; Chen, C.G.; Peng, Y.; Bai, X.B.; Miao, L. Substantial thermoelectric enhancement achieved by manipulating the band structure and dislocations in Ag and La co-doped SnTe. *J. Adv. Ceram.* **2021**, *10*, 860–870. [[CrossRef](#)]
7. Rogl, G.; Grytsiv, A.; Anbalagan, R.; Bursik, J.; Kerber, M.; Schafner, E.; Zehetbauer, M.; Bauer, E.; Rogl, P. Direct SPD-processing to achieve high-ZT skutterudites. *Acta Mater.* **2018**, *159*, 352–363. [[CrossRef](#)]
8. Zheng, Y.P.; Zou, M.C.; Zhang, W.Y.; Yi, D.; Lan, J.L.; Nan, C.-W.; Lin, Y.-H. Electrical and thermal transport behaviours of high-entropy perovskite thermoelectric oxides. *J. Adv. Ceram.* **2021**, *10*, 377–384. [[CrossRef](#)]
9. Slack, G.A. *CRC Handbook of Thermoelectric*; CRC Press: Boca Raton, FL, USA, 1995; pp. 407–440.
10. Xia, X.; Huang, X.; Li, X.; Gu, M.; Qiu, P.; Liao, J.; Tang, Y.; Bai, S.; Chen, L. Preparation and structural evolution of Mo/SiO_x protective coating on CoSb₃-based filled skutterudite thermoelectric material. *J. Alloys Compd.* **2014**, *604*, 94–99. [[CrossRef](#)]
11. Drevet, R.; Aranda, L.; Petitjean, C.; David, N.; Veys-Renaux, D.; Berthod, P. Oxidation Behavior of the Skutterudite Material Ce_{0.75}Fe₃CoSb₁₂. *Oxid. Met.* **2019**, *91*, 767–779. [[CrossRef](#)]
12. Schmidt, R.D.; Case, E.D.; Ni, J.E.; Sakamoto, J.S.; Trejo, R.M.; Lara-Curzio, E.; Payzant, E.A.; Kirkham, M.J.; Peascoe-Meisner, R.A. The temperature dependence of thermal expansion for p-type Ce_{0.9}Fe_{3.5}Co_{0.5}Sb₁₂ and n-type Co_{0.95}Pd_{0.05}Te_{0.05}Sb₃ skutterudite thermoelectric materials. *Philos. Mag.* **2012**, *92*, 1261–1286. [[CrossRef](#)]
13. Li, Y.; Li, C.; Wang, B.; Li, W.; Che, P. A comparative study on the thermoelectric properties of CoSb₃ prepared by hydrothermal and solvothermal route. *J. Alloys Compd.* **2019**, *772*, 770–774. [[CrossRef](#)]
14. Ghosh, S.; Shankar, G.; Karati, A.; Werbach, K.; Rogl, G.; Rogl, P.; Bauer, E.; Murty, B.S.; Suwas, S.; Mallik, R.C. Enhanced Thermoelectric Performance in the Ba_{0.3}Co₄Sb₁₂/InSb Nanocomposite Originating from the Minimum Possible Lattice Thermal Conductivity. *ACS Appl. Mater. Interfaces* **2020**, *12*, 48729–48740. [[CrossRef](#)]
15. Wang, S.; Salvador, J.R.; Yang, J.; Wei, P.; Duan, B.; Yang, J. High-performance n-type Yb_xCo₄Sb₁₂: From partially filled skutterudites towards composite thermoelectrics. *NPG Asia Mater.* **2016**, *8*, e285. [[CrossRef](#)]
16. Rogl, G.; Grytsiv, A.; Rogl, P.; Peranio, N.; Bauer, E.; Zehetbauer, M.; Eibl, O. n-Type skutterudites (R;Ba;Yb)_yCo₄Sb₁₂ (R=Sr; La; Mm; DD.; SrMm; SrDD) approaching ZT≈2.0. *Acta Mater.* **2014**, *63*, 30–43. [[CrossRef](#)]
17. Zong, P.-A.; Hanus, R.; Dylla, M.; Tang, Y.; Liao, J.; Zhang, Q.; Snyder, G.J.; Chen, L. Skutterudite with graphene-modified grain-boundary complexion enhances zT enabling high-efficiency thermoelectric device. *Energy Environ. Sci.* **2017**, *10*, 183–191. [[CrossRef](#)]
18. Liu, Z.-Y.; Zhu, J.-L.; Tong, X.; Niu, S.; Zhao, W.-Y. A review of CoSb₃-based skutterudite thermoelectric materials. *J. Adv. Ceram.* **2020**, *9*, 647–673. [[CrossRef](#)]
19. Zhu, J.; Liu, Z.; Tong, X.; Xia, A.; Xu, D.; Lei, Y.; Yu, J.; Tang, D.; Ruan, X.; Zhao, W. Synergistic Optimization of Electrical-Thermal-Mechanical Properties of the In-Filled CoSb₃ Material by Introducing Bi_{0.5}Sb_{1.5}Te₃ Nanoparticles. *ACS Appl. Mater. Interfaces* **2021**, *13*, 23894–23904. [[CrossRef](#)]
20. Zheng, Y.J.; Wang, A.Q.; Jia, X.P.; Wang, F.B.; Yang, A.L.; Huang, H.L.; Zuo, G.H.; Wang, L.B.; Deng, L. Optimization of thermoelectric properties of CoSb₃ materials by increasing the complexity of chemical structure. *J. Alloys Compd.* **2020**, *843*, 156063. [[CrossRef](#)]
21. Matsubara, M.; Asahi, R. Optimization of filler elements in CoSb₃-based skutterudites for high-performance n-type thermoelectric materials. *J. Electron. Mater.* **2015**, *45*, 1669–1678. [[CrossRef](#)]
22. Tong, X.; Liu, Z.Y.; Zhu, J.L.; Yang, T.; Wang, Y.G.; Xia, A.L. Research progress of p-type Fe-based skutterudite thermoelectric materials. *Front. Mater. Sci.* **2021**, *15*, 317–333. [[CrossRef](#)]
23. Ghosh, S.; Valiyaveetil, S.M.; Shankar, G.; Maity, T.; Chen, K.-H.; Biswas, K.; Suwas, S.; Mallik, R.C. Enhanced thermoelectric properties of in-filled Co₄Sb₁₂ with InSb nano-inclusions. *ACS Appl. Energy Mater.* **2020**, *3*, 635–646. [[CrossRef](#)]
24. Zhao, W.Y.; Liu, Z.Y.; Sun, Z.G.; Zhang, Q.J.; Wei, P.; Mu, X.; Zhou, H.Y.; Li, C.C.; Ma, S.F.; He, D.Q.; et al. Superparamagnetic enhancement of thermoelectric performance. *Nature* **2017**, *549*, 247–251. [[CrossRef](#)]
25. Zhao, W.Y.; Liu, Z.Y.; Wei, P.; Zhang, Q.J.; Zhu, W.T.; Su, X.L.; Tang, X.F.; Yang, J.H.; Liu, Y.; Shi, J.; et al. Magnetoelectric interaction and transport behaviors in magnetic nanocomposite thermoelectric materials. *Nat. Nanotechnol.* **2017**, *12*, 55–61. [[CrossRef](#)]
26. Liu, Z.Y.; Zhu, J.L.; Wei, P.; Zhu, W.T.; Zhao, W.Y.; Xia, A.L.; Xu, D.; Lei, Y.; Yu, J. Candidate for magnetic doping agent and high-temperature thermoelectric performance enhancer: Hard magnetic m-type BaFe₁₂O₁₉ nanometer suspension. *ACS Appl. Mater. Interfaces* **2019**, *11*, 45875–45884. [[CrossRef](#)]
27. Liang, T.; Su, X.; Yan, Y.; Zheng, G.; Zhang, Q.; Chi, H.; Tang, X.; Uher, C. Ultra-fast synthesis and thermoelectric properties of Te doped skutterudites. *J. Mater. Chem. A* **2014**, *2*, 17914–17918. [[CrossRef](#)]
28. Pillaca, M.; Harder, O.; Miller, W.; Gille, P. Forced convection by Inclined Rotary Bridgman method for growth of CoSb₃ and FeSb₂ single crystals from Sb-rich solutions. *J. Cryst. Grow.* **2017**, *475*, 346–353. [[CrossRef](#)]
29. Caillat, T.; Fleurial, J.-P.; Borshchevsky, A. Bridgman-solution crystal growth and characterization of the skutterudite compounds CoSb₃ and RhSb₃. *J. Cryst. Grow.* **1996**, *166*, 722–726. [[CrossRef](#)]
30. Wang, H.; Li, S.; Li, X.; Zhong, H. Microstructure and thermoelectric properties of doped p-type CoSb₃ under TGZM effect. *J. Cryst. Grow.* **2017**, *466*, 56–63. [[CrossRef](#)]
31. Qin, Z.; Cai, K.F.; Chen, S.; Du, Y. Preparation and electrical transport properties of In filled and Te-doped CoSb₃ skutterudite. *J. Mater. Sci.* **2013**, *24*, 4142–4147. [[CrossRef](#)]

32. Kumar, M.U.; Swetha, R.; Kumari, L. Structural and Optical Studies on Strontium-Filled CoSb₃ Nanoparticles Via a Solvo-/Hydrothermal Method. *J. Electron. Mater.* **2021**, *50*, 1735–1741. [[CrossRef](#)]
33. Gharleghi, A.; Pai, Y.-H.; Lin, F.-H.; Liu, C.-J. Low thermal conductivity and rapid synthesis of n-type cobalt skutterudite via a hydrothermal method. *J. Mater. Chem. C* **2014**, *2*, 4213–4220. [[CrossRef](#)]
34. Dresselhaus, M.S.; Chen, G.; Tang, M.Y.; Yang, R.G.; Lee, H.; Wang, D.Z.; Ren, Z.F.; Fleurial, J.P.; Gogna, P. New Directions for Low-Dimensional Thermoelectric Materials. *Adv. Mater.* **2007**, *19*, 1043–1053. [[CrossRef](#)]
35. Yu, J.; Zhao, W.-Y.; Wei, P.; Tang, D.-G.; Zhang, Q.-J. Effects of excess Sb on thermoelectric properties of barium and indium double-filled iron-based p-type skutterudite materials. *J. Electron. Mater.* **2012**, *41*, 1414–1420. [[CrossRef](#)]
36. Wan, S.; Huang, X.; Qiu, P.; Shi, X.; Chen, L. Compound Defects and Thermoelectric Properties of Self-Charge Compensated Skutterudites Se_yCo₄Sb_{12-x}Se_x. *ACS Appl. Mater. Interfaces* **2017**, *9*, 22713–22724. [[CrossRef](#)]
37. Yang, K.; Cheng, H.; Hng, H.H.; Ma, J.; Mi, J.L.; Zhao, X.B.; Zhu, T.J.; Zhang, Y.B. Synthesis and thermoelectric properties of double-filled skutterudites Ce_yYb_{0.5-y}Fe_{1.5}Co_{2.5}Sb₁₂. *J. Alloys Compd.* **2009**, *467*, 528–532. [[CrossRef](#)]
38. Bao, X.; Wu, Z.H.; Xie, H.Q. Enhanced thermoelectric properties of CoSb₃-based skutterudites by filling Se as electronegative element. *Mater. Res. Express* **2018**, *6*, 2053. [[CrossRef](#)]
39. Wan, S.; Qiu, P.F.; Huang, X.Y.; Song, Q.F.; Bai, S.Q.; Shi, X.; Chen, L.D. Synthesis and Thermoelectric Properties of Charge-Compensated SyPd_xCo_{4-x}Sb₁₂ Skutterudites. *ACS Appl. Mater. Interfaces* **2017**, *10*, 625–634. [[CrossRef](#)]
40. Su, X.; Li, H.; Wang, G.; Chi, H.; Zhou, X.; Tang, X.; Zhang, Q.; Uher, C. Structure and Transport Properties of Double-Doped CoSb_{2.75}Ge_{0.25-x}Te_x (x = 0.125–0.20) with in Situ Nanostructure. *Chem. Mater.* **2011**, *23*, 2948–2955. [[CrossRef](#)]
41. Taha, M.A.; Youness, R.A.; Zawrah, M.F. Review on nanocomposites fabricated by mechanical alloying. *Int. J. Min. Met. Mater.* **2019**, *26*, 1047–1058. [[CrossRef](#)]
42. Ur, S.-C.; Kwon, J.-C.; Kim, I.-H. Thermoelectric properties of Fe-doped CoSb₃ prepared by mechanical alloying and vacuum hot pressing. *J. Alloys Compd.* **2007**, *442*, 358–361. [[CrossRef](#)]
43. Liu, W.-S.; Zhang, B.-P.; Li, J.-F.; Zhao, L.-D. Thermoelectric property of fine-grained CoSb₃ skutterudite compound fabricated by mechanical alloying and spark plasma sintering. *J. Phys. D* **2007**, *40*, 566–572. [[CrossRef](#)]
44. Lin, B.L.; Tang, X.F.; Qi, Q.; Zhang, Q.J. Preparation and thermal transport properties of CoSb₃ nano-compounds. *Acta Phys. Sin.* **2004**, *53*, 3130–3135.
45. Trivedi, V.; Battabyal, M.; Balasubramanian, P.; Muralikrishna, G.M.; Jain, P.K.; Gopalan, R. Microstructure and doping effect on the enhancement of the thermoelectric properties of Ni doped Dy filled CoSb₃ skutterudites. *Sustain. Energy Fuels* **2018**, *2*, 2687–2697. [[CrossRef](#)]
46. Rogl, G.; Grytsiv, A.; Yubuta, K.; Puchegger, S.; Bauer, E.; Raju, C.; Mallik, R.C.; Rogl, P. In-doped multifilled n-type skutterudites with ZT=1.8. *Acta Mater.* **2015**, *95*, 201–211. [[CrossRef](#)]
47. Thomas, R.; Rao, A.; Chauhan, N.S.; Vishwakarma, A.; Singh, N.K.; Soni, A. Melt spinning: A rapid and cost effective approach over ball milling for the production of nanostructured p-type Si₈₀Ge₂₀ with enhanced thermoelectric properties. *J. Alloys Compd.* **2019**, *781*, 344–350. [[CrossRef](#)]
48. Kim, T.S.; Chun, B.S. Thermoelectric Properties of n-Typen-type 90%Bi₂Te₃+10%Bi₂Se₃ Thermoelectric Materials Produced by Melt Spinning Method and Sintering. *Mater. Sci. Forum* **2007**, *534–536*, 161–164. [[CrossRef](#)]
49. Jie, Q.; Zhou, J.; Dimitrov, I.K. Thermoelectric properties of non-equilibrium synthesized Ce_{0.9}Fe₃CoSb₁₂ filled skutterudites. *MRS Proc.* **2010**, *1267*, 55–60. [[CrossRef](#)]
50. Son, G.; Lee, K.H.; Choi, S.-M. Enhanced Thermoelectric Properties of Melt-Spun p-Type Yb_{0.9}Fe₃CoSb₁₂. *J. Electron. Mater.* **2016**, *46*, 2839–2843. [[CrossRef](#)]
51. Tan, H.; Guo, L.; Wang, G.; Wu, H.; Shen, X.; Zhang, B.; Lu, X.; Wang, G.; Zhang, X.; Zhou, X. Synergistic Effect of Bismuth and Indium Codoping for High Thermoelectric Performance of Melt Spinning SnTe Alloys. *ACS Appl. Mater. Interfaces* **2019**, *11*, 23337–23345. [[CrossRef](#)]
52. Thompson, D.R.; Liu, C.; Ellison, N.D.; Salvador, J.R.; Meyer, M.S.; Haddad, D.B.; Wang, H.; Cai, W. Improved thermoelectric performance of n-type Ca and Ca-Ce filled skutterudites. *J. Appl. Phys.* **2014**, *116*, 243701. [[CrossRef](#)]
53. Sun, H.; Jia, X.; Lv, P.; Deng, L.; Guo, X.; Zhang, Y.; Sun, B.; Liu, B.; Ma, H. Improved thermoelectric performance of Te-doped and CNT dispersed CoSb₃ skutterudite bulk materials via HTHP. *RSC Adv.* **2015**, *5*, 61324–613429. [[CrossRef](#)]
54. Sun, H.; Jia, X.; Deng, L.; Lv, P.; Guo, X.; Sun, B.; Zhang, Y.; Liu, B.; Ma, H. Impacts of both high pressure and Te-Se double-substituted skutterudite on the thermoelectric properties prepared by HTHP. *J. Alloys Compd.* **2014**, *615*, 1056–1059. [[CrossRef](#)]
55. Han, X.; Wang, L.B.; Li, D.N.; Deng, L.; Jia, X.P.; Ma, H.A. Effects of pressure and ions doping on the optimization of double filled CoSb₃ thermoelectric materials. *Mater. Lett.* **2019**, *237*, 49–52. [[CrossRef](#)]
56. Kong, L.; Jia, X.; Zhang, Y.; Sun, B.; Liu, B.; Liu, H.; Wang, C.; Liu, B.; Chen, J.; Ma, H. N-type Ba_{0.3}Ni_{0.15}Co_{3.85}Sb₁₂ skutterudite: High pressure processing technique and thermoelectric properties. *J. Alloys Compd.* **2018**, *734*, 36–42. [[CrossRef](#)]
57. Jiang, Y.; Jia, X.; Ma, H. The thermoelectric properties of CoSb₃ compound doped with Te and Sn synthesized at different pressure. *Mod. Phys. Lett. B* **2017**, *31*, 1750261. [[CrossRef](#)]
58. Deng, L.; Jia, X.P.; Su, T.C.; Jiang, Y.P.; Zheng, S.Z.; Guo, X.; Ma, H.A. The enhanced thermoelectric properties of Ba_{0.25}Pb_{0.05}Co₄Sb_{11.5}Te_{0.5} alloys prepared by HPHT at different pressure. *Mater. Lett.* **2011**, *65*, 1582–1594. [[CrossRef](#)]

59. De, V.J.C.; Lee, D.; Shin, H.; Namuco, S.B.; Hwang, I.; Sarmago, R.V.; Song, J.H. Influence of deposition conditions on the growth of micron-thick highly c-axis textured superconducting $\text{GdBa}_2\text{Cu}_3\text{O}_{7-\delta}$ films on SrTiO_3 (100). *J. Vac. Sci. Technol.* **2018**, *36*, 031506.
60. Sarath, K.S.R.; Alyamani, A.; Graff, J.W.; Tritt, T.M.; Alshareef, H.N. Pulsed laser deposition and thermoelectric properties of In- and Yb-doped CoSb_3 skutterudite thin films. *J. Mater. Res.* **2011**, *26*, 1836–1841. [[CrossRef](#)]
61. Jelínek, M.; Zeipl, R.; Kocourek, T.; Remsa, J.; Navrátil, J. Thermoelectric nanocrystalline YbCoSb laser prepared layers. *Appl. Phys. A* **2016**, *122*, 155. [[CrossRef](#)]
62. Masarrat, A.; Bhogra, A.; Meena, R.; Bala, M.; Singh, R.; Barwal, V.; Dong, C.L.; Chen, C.L.; Som, T.; Kumar, A.; et al. Effect of Fe ion implantation on the thermoelectric properties and electronic structures of CoSb_3 thin films. *RSC Adv.* **2019**, *9*, 36113–36122. [[CrossRef](#)]
63. Kelly, P.J.; Arnell, R.D. Magnetron sputtering: A review of recent developments and applications. *Vacuum* **2000**, *56*, 159–172. [[CrossRef](#)]
64. Fan, P.; Wei, M.; Zheng, Z.-H.; Zhang, X.-H.; Ma, H.-L.; Luo, J.-T.; Liang, G.-X. Effects of Ag-doped content on the microstructure and thermoelectric properties of CoSb_3 thin films. *Thin Solid Films* **2019**, *679*, 49–54. [[CrossRef](#)]
65. Zheng, Z.-H.; Li, F.; Li, F.; Li, Y.-Z.; Fan, P.; Luo, J.-T.; Liang, G.-X.; Fan, B.; Zhong, A.-H. Thermoelectric properties of co-sputtered CoSb_3 thin films as a function of stoichiometry. *Thin Solid Films* **2017**, *632*, 88–92. [[CrossRef](#)]
66. Li, Y.D.; Zheng, Z.H.; Fan, P.; Luo, J.T.; Liang, G.X.; Huang, B.X. Thermoelectric Characterization of Ti and In Double-Doped Cobalt Antimony Thin Films. *Mater. Sci. Forum.* **2016**, *847*, 143–147. [[CrossRef](#)]
67. Zhou, J.M. Development of molecular beam epitaxy in China. *Physics* **2021**, *50*, 843–848.
68. Goodhue, W.G.; Reeder, R.E.; Vineis, C.J.; Calawa, S.D.; Dauplaise, H.M.; Vangala, S.; Walsh, M.P.; Harman, T.C. High-output-power densities from molecular beam epitaxy grown n- and p-type PbTeSe -based thermoelectrics via improved contact metallization. *J. Appl. Phys.* **2012**, *111*, 104501. [[CrossRef](#)]
69. Daniel, M.V.; Brombacher, C.; Beddies, G.; Jöhrmann, N.; Hietschold, M.; Johnson, D.C.; Aabdin, Z.; Peranio, N.; Eibl, O.; Albrecht, M. Structural properties of thermoelectric CoSb_3 skutterudite thin films prepared by molecular beam deposition. *J. Alloys Compd.* **2015**, *624*, 216–225. [[CrossRef](#)]
70. Peranio, N.; Eibl, O.; Bäßler, S.; Nielsch, K.; Klobes, B.; Hermann, R.P.; Daniel, M.; Albrecht, M.; Görlitz, H.; Pacheco, V.; et al. From thermoelectric bulk to nanomaterials: Current progress for Bi_2Te_3 and CoSb_3 . *Phys. Status Solidi A* **2016**, *213*, 739–749. [[CrossRef](#)]
71. Makogon, Y.N.; Pavlova, E.P.; Sidorenko, S.I.; Shkarban', R.A.; Figurnaya, E.V. Effect of Sb content on the phase composition of CoSb_x nanofilms grown on a heated substrate. *Inorg. Mater.* **2014**, *50*, 431–436. [[CrossRef](#)]
72. Zhang, Q.; Fan, J.; Fan, W.; Zhang, H.; Chen, S.; Wu, Y.; Tang, X.; Xu, B. Energy-Efficient Synthesis and Superior Thermoelectric Performance of Sb-doped $\text{Mg}_2\text{Si}_{0.3}\text{Sn}_{0.7}$ Solid Solutions by Rapid Thermal Explosion. *Mater. Res. Bull.* **2020**, *128*, 110885. [[CrossRef](#)]
73. Liu, R.; Tan, X.; Ren, G.; Liu, Y.; Zhou, Z.; Liu, C.; Lin, Y.; Nan, C. Enhanced Thermoelectric Performance of Te-Doped $\text{Bi}_2\text{Se}_{3-x}\text{Te}_x$ Bulks by Self-Propagating High-Temperature Synthesis. *Crystals* **2017**, *7*, 257. [[CrossRef](#)]
74. Roslyakov, S.I.; Kovalev, D.Y.; Rogachev, A.S. Solution Combustion Synthesis: Dynamics of Phase Formation for Highly Porous Nickel. *Dokl. Phys. Chem.* **2013**, *449*, 48–51. [[CrossRef](#)]
75. Su, X.; Fu, F.; Yan, Y.; Zheng, G.; Liang, T.; Zhang, Q.; Cheng, X.; Yang, D.; Chi, H.; Tang, X.; et al. Self-propagating high-temperature synthesis for compound thermoelectrics and new criterion for combustion processing. *Nat. Commun.* **2014**, *5*, 4908. [[CrossRef](#)]
76. Xing, Y.; Liu, R.; Sun, Y.-Y.; Chen, F.; Zhao, K.; Zhu, T.; Bai, S.; Chen, L. Self-propagation high-temperature synthesis of half-Heusler thermoelectric materials: reaction mechanism and applicability. *J. Mater. Chem.* **2018**, *6*, 19470–19478. [[CrossRef](#)]
77. Xing, Y.F.; Liu, R.H.; Liao, J.C.; Zhang, Q.H.; Xia, X.G.; Wang, C.; Huang, H.; Chu, J.; Gu, M.; Zhu, T.J.; et al. High-efficiency half-Heusler thermoelectric modules enabled by self-propagating synthesis and topologic structure optimization. *Energy Environ. Sci.* **2019**, *12*, 3390–3399. [[CrossRef](#)]
78. Kruszewski, M.J.; Cymerman, K.; Zybala, R.; Chmielewski, M.; Kowalczyk, M.; Zdunek, J.; Ciupiński, Ł. High homogeneity and ultralow lattice thermal conductivity in Se/Te-doped skutterudites obtained by self-propagating high-temperature synthesis and pulse plasma sintering. *J. Alloys Compd.* **2022**, *909*, 164796. [[CrossRef](#)]
79. Biswas, K.; Muir, S.; Subramanian, M.A. Rapid microwave synthesis of indium filled skutterudites: An energy efficient route to high performance thermoelectric materials. *Mater. Res. Bull.* **2011**, *46*, 2288–2290. [[CrossRef](#)]
80. Thirupathi, K.; Raghuraman, S.; Mohan, R.R. Densification Studies on Aluminum-Based Brake Lining Composite Processed by Microwave and Spark Plasma Sintering. *Powder Metall. Met. Ceram.* **2021**, *60*, 44–51. [[CrossRef](#)]
81. Lei, Y.; Gao, W.; Zheng, R.; Li, Y.; Wan, R.; Chen, W.; Ma, L.; Zhou, H.; Chu, P.K. Rapid synthesis; microstructure; and thermoelectric properties of skutterudites. *J. Alloys Compd.* **2019**, *806*, 537–542. [[CrossRef](#)]
82. Lei, Y.; Gao, W.; Zheng, R.; Li, Y.; Chen, W.; Zhang, L.; Wan, R.; Zhou, H.; Liu, Z.; Chu, P.K. Ultrafast Synthesis of Te-Doped CoSb_3 with Excellent Thermoelectric Properties. *ACS Appl. Energy Mater.* **2019**, *2*, 4477–4485. [[CrossRef](#)]
83. Kitchen, H.J.; Vallance, S.R.; Kennedy, J.L.; Tapia, R.N.; Carassiti, L.; Harrison, A.; Whittaker, A.G.; Drysdale, T.D.; Kingman, S.W.; Gregory, D.H. Modern microwave methods in solid-state inorganic materials chemistry: From fundamentals to manufacturing. *Chem. Rev.* **2014**, *114*, 1170–1206. [[CrossRef](#)] [[PubMed](#)]

84. Lei, Y.; Gao, W.S.; Li, Y.; Wan, R.D.; Chen, W.; Zheng, R.; Ma, L.Q.; Zhou, H.W. Structure and thermoelectric performance of Ti-filled and Te-doped skutterudite $Ti_xCo_4Sb_{11.5}Te_{0.5}$ bulks fabricated by combination of microwave synthesis and spark plasma sintering. *Mater. Lett.* **2018**, *233*, 166–169. [[CrossRef](#)]
85. Zehetbauer, M.J.; Zhu, Y.T. *Bulk Nanostructured Materials*; VCH Wiley: Weinheim, Germany, 2009.
86. Rogl, G.; Grytsiv, A.; Rogl, P.; Royanian, E.; Bauer, E.; Horky, J.; Setman, D.; Schafner, E.; Zehetbauer, M. Dependence of thermoelectric behaviour on severe plastic deformation parameters: A case study on p-type skutterudite $DD_{0.60}Fe_3CoSb_{12}$. *Acta Mater.* **2013**, *61*, 6778–6789. [[CrossRef](#)]
87. Rogl, G.; Grytsiv, A.; Heinrich, P.; Bauer, E.; Kumar, P.; Peranio, N.; Eibl, O.; Horky, J.; Zehetbauer, M.; Rogl, P. New bulk p-type skutterudites $DD_{0.7}Fe_{2.7}Co_{1.3}Sb_{12-x}X_x$ ($X = Ge, Sn$) reaching $ZT > 1.3$. *Acta Mater.* **2015**, *91*, 227–238. [[CrossRef](#)]
88. Rogl, G.; Aabdin, Z.; Schafner, E. Effect of HPT processing on the structure, thermoelectric and mechanical properties of $Sr_{0.07}Ba_{0.07}Yb_{0.07}Co_4Sb_{12}$. *J. Alloys Compd.* **2012**, *537*, 183–189. [[CrossRef](#)]
89. Rogl, G.; Ghosh, S.; Renk, O.; Yubuta, K.; Grytsiv, A.; Schafner, E.; Zehetbauer, M.; Mallik, R.C.; Bauer, E.; Rogl, P. HPT production of large bulk skutterudites. *J. Alloys Compd.* **2021**, *854*, 156678. [[CrossRef](#)]